

Backscatter analysis based algorithms for increasing transmission through highly-scattering random media using phase-only modulated wavefronts

Curtis Jin*, Raj Rao Nadakuditi, Eric Michielssen and Stephen C. Rand

Dept. of EECS, University of Michigan, Ann Arbor, Michigan 48109-2122, USA

**Corresponding author: jsirius@umich.edu*

arXiv:1402.3015v2 [physics.optics] 20 Jun 2014

Recent theoretical and experimental advances have shed light on the existence of so-called ‘perfectly transmitting’ wavefronts with transmission coefficients close to 1 in strongly backscattering random media. These perfectly transmitting eigen-wavefronts can be synthesized by spatial amplitude and phase modulation.

Here, we consider the problem of transmission enhancement using phase-only modulated wavefronts. Motivated by biomedical applications in which it is not possible to measure the transmitted fields, we develop physically realizable iterative and non-iterative algorithms for increasing the transmission through such random media using backscatter analysis. We theoretically show that, despite the phase-only modulation constraint, the non-iterative algorithms will achieve at least about $25\pi\% \approx 78.5\%$ transmission with very high probability, assuming that there is at least one perfectly transmitting eigen-wavefront and that the singular vectors of the transmission matrix obey a maximum entropy principle so that they are isotropically random.

We numerically analyze the limits of phase-only modulated transmission in 2-D with fully spectrally accurate simulators and provide rigorous numerical evidence confirming our theoretical prediction in random media with periodic boundary conditions that is composed of hundreds of thousands of non-absorbing scatterers. We show via numerical simulations that the iterative algorithms we have developed converge rapidly, yielding highly transmitting wavefronts using relatively few measurements of the backscatter field. Specifically, the best performing iterative algorithm yields $\approx 70\%$ transmission using just 15 – 20 measurements in the regime where the non-iterative algorithms yield $\approx 78.5\%$ transmission but require measuring the entire modal reflection matrix. Our theoretical analysis and rigorous numerical results validate our prediction that phase-only modulation with a given number of spatial modes will yield higher transmission than amplitude and phase modulation with half as many modes. © 2022 Optical Society of America

OCIS codes: 030.6600

1. Introduction

Multiple scattering by randomly placed particles frustrates the passage of light through ‘opaque’ materials such as turbid water, white paint, and egg shells. Thanks to the theoretical work of Dorokhov [8], Barnes and Pendry et al. [2, 28], and others [3, 25], as well as the breakthrough experiments of Vellekoop and Mosk [43, 44] and others [1, 6, 7, 19, 20, 29, 31, 37, 40], we now understand that even though a normally incident wavefront will barely

propagate through a thick slab of such media [16], a small number of eigen-wavefronts exist that exhibit a transmission coefficient close to one and hence propagate through the slab without significant loss.

In highly scattering random media composed of non-absorbing scatterers, these ‘perfectly transmitting’ eigen-wavefronts are the right singular vectors of the modal transmission matrix with singular values (or transmission coefficients) close to 1. Thus, if the modal transmission matrix were measured using the techniques described in [19, 20, 29, 31], one could compute the pertinent singular vector and synthesize a highly transmitting eigen-wavefront via spatial amplitude and phase modulation. The task of amplitude and phase modulating an optical wavefront is not, however, trivial. Calibration and alignment issues prevent the use of two independent spatial light modulators in series that separately modulate the signal amplitude and phase. A viable option is to use the innovative method developed by van Putten et al. in [41] for full spatial phase and amplitude control using a twisted nematic LCD combined with a spatial filter.

In a recent paper [17, 18], we assumed that amplitude and phase modulation was feasible, and developed iterative, physically-realizable algorithms for synthesizing highly transmitting eigen-wavefronts using just a few measurements of the backscatter field. We showed that the algorithms converge rapidly and achieve 95% transmission using about 5 – 10 measurements. Our focus on constructing highly transmitting eigen-wavefronts by using the information in the backscatter field was motivated by biomedical applications, where it is often impossible to measure transmitted fields. Our work will be most helpful in settings where it is desirable to increase the amount of light transmitted through an intervening scattering medium such as in photodynamic therapy where a photosynthesizing agent on exposure to light produces a form of oxygen that can kill neighboring (cancerous) cells [9]. Another promising application is in photoacoustic imaging [45] which exploits the photoacoustic effect whereby light is converted into heat by absorbing scatterers and the subsequent thermoelastic expansion produces wideband ultrasonic emissions which can be detected by ultrasonic transducers to form images. Recent breakthrough works have taken this a step further by exploiting the photoacoustic effect to focus light within the medium [4, 21]. Since the strength of the photoacoustic effect is proportional to the scattered light intensity at the light absorber, one might reasonably expect that algorithms, such as ours, that can increase the amount of transmitted light through a medium can help improve the penetration depth of photoacoustic imaging (or photoacoustic imaging guided focusing) by inducing stronger photoacoustic signals from deeper in the medium.

Here, we place ourselves in the setting where we seek to increase transmission via backscatter analysis but are restricted to phase-only modulation. The phase-only modulation constraint was initially motivated by the simplicity of the resulting experimental setup (see

Fig. 1) and the commercial availability of finely calibrated phase-only spatial light modulators (SLMs) (e.g. the PLUTO series from Holoeye). As we shall shortly see there is another engineering advantage conferred by these methods. We do not, however, expect to achieve perfect transmission using phase-only modulation as is achievable by amplitude and phase modulation. However, we theoretically show that we can expect to get at least (about) $25\pi\% \approx 78.5\%$ provided that 1) the system modal reflection (or transmission) matrix is known, 2) its right singular vectors obey a maximum entropy principle by being isotropically random, and 3) full amplitude and phase modulation permits at least one perfectly transmitting wavefront. We also develop iterative, physically realizable algorithms for transmission maximization that utilize backscatter analysis to produce a highly transmitting phase-only modulated wavefront in just a few iterations. These rapidly converging algorithms build on the ideas developed in [17, 18] by incorporating the phase-only constraint. An additional advantage conferred by these rapidly converging algorithms is that they might facilitate their use in applications where the duration in which the modal transmission or reflection matrix can be assumed to be constant is relatively small compared to the time it would take to make all measurements needed to estimate the modal transition or reflection matrix or in settings where a near-optimal solution obtained fast is preferable to the optimal solution that takes many more measurements to compute. As in [18], the iterative algorithms we have developed retain the feature that they allow the number of modes being controlled via an SLM in experiments to be increased without increasing the number of measurements that have to be made.

We numerically analyze the limits of phase-only modulated transmission in 2-D with fully spectrally accurate simulators and provide rigorous numerical evidence confirming our theoretical prediction in random media with periodic boundary conditions that is composed of hundreds of thousands of non-absorbing scatterers. Specifically, we show that the best performing iterative algorithm yields $\approx 70\%$ transmission using just 15 – 20 measurements in the regime where the non-iterative algorithms yield $\approx 78.5\%$ transmission.

This theoretical prediction brings into sharp focus an engineering advantage to phase-only modulation relative to amplitude and phase modulation that we did not anticipate when we embarked on this line of inquiry. The clever idea in van Putten et al’s work was to use spatial filtering to combine four neighboring pixels into one superpixel and then independently modulate the phase and the amplitude of light at each superpixel. This implies that an SLM with M pixels can control at most $M/4$ spatial modes. For a given aperture, combining neighboring pixels into one super pixel corresponds to passing the entire wavefront into a spatial low pass filter. We argue that in critically or undersampled scenarios phase-only measurements permit the design of more highly transmitting wavefronts than amplitude-phase measurements that use the idea of van Putten et al.

For highly scattering random media, our numerical results in Section 7, suggest that undersampling the spatial modes by 75% will reduce the average amount of transmission by between 65–75%. In contrast, our theoretical results in Section 5 show that controlling all M spatial modes using phase-only modulation will reduce the average amount of transmission by at most 30%. Thus, we can, on average, achieve higher transmission with phase-only modulation using all the pixels in an SLM than by (integer-valued) undersampling of the pixels to implement amplitude and phase modulation! The paper is organized as follows. We describe our setup in Section 2. We discuss the problem of transmission maximization using phase-only modulated wavefronts in Section 3. We describe physically realizable, non-iterative and iterative algorithms for transmission maximization in Section 4 and in Section 6, respectively. We identify fundamental limits of phase-only modulated transmission in Section 5, validate the predictions and the rapid convergence behavior of the iterative algorithms in Section 7, and summarize our findings in Section 8.

2. Setup

We study scattering from a two-dimensional (2D) periodic slab of thickness L and periodicity D . The slab's unit cell occupies the space $0 \leq x < D$ and $0 \leq y < L$ (Fig. 2) and contains N_c infinite and z -invariant circular cylinders of radius r that are placed randomly within the cell and assumed either perfect electrically conducting (PEC) or dielectric with refractive index n_d . Care is taken to ensure the cylinders do not overlap. All fields are TM_z polarized: electric fields in the $y < 0$ ($i = 1$) and $y > L$ ($i = 2$) halfspaces are denoted $\underline{e}_i(\underline{\rho}) = e_i(\underline{\rho})\hat{z}$. These fields (complex) amplitudes $e_i(\underline{\rho})$ can be decomposed in terms of $+y$ and $-y$ propagating waves as $e_i(\underline{\rho}) = e_i^+(\underline{\rho}) + e_i^-(\underline{\rho})$, where

$$e_i^\pm(\underline{\rho}) = \sum_{n=-N}^N h_n a_{i,n}^\pm e^{-jk_n^\pm \cdot \underline{\rho}}. \quad (1)$$

In the above expression, $\underline{\rho} = x\hat{x} + y\hat{y} \equiv (x, y)$, $\underline{k}_n^\pm = k_{n,x}\hat{x} \pm k_{n,y}\hat{y} \equiv (k_{n,x}, \pm k_{n,y})$, $k_{n,x} = 2\pi n/D$, $k_{n,y} = 2\pi\sqrt{(1/\lambda)^2 - (n/D)^2}$, λ is the wavelength, and $h_n = \sqrt{\|\underline{k}_n^\pm\|_2/k_{n,y}}$ is a power-normalizing coefficient. We assume $N = \lfloor D/\lambda \rfloor$, i.e., we only model propagating waves and denote $M = 2N + 1$. The modal coefficients $a_{i,n}^\pm$, $i = 1, 2$; $n = -N, \dots, N$ are related by the scattering matrix

$$\begin{bmatrix} \underline{a}_1^- \\ \underline{a}_2^+ \end{bmatrix} = \underbrace{\begin{bmatrix} S_{11} & S_{12} \\ S_{21} & S_{22} \end{bmatrix}}_{=:S} \begin{bmatrix} \underline{a}_1^+ \\ \underline{a}_2^- \end{bmatrix}, \quad (2)$$

where $\underline{a}_i^\pm = [a_{i,-N}^\pm \ \dots \ a_{i,-1}^\pm \ a_{i,0}^\pm \ a_{i,1}^\pm \ \dots \ a_{i,N}^\pm]^T$ and T denotes transposition. In what follows, we assume that the slab is only excited from the $y < 0$ halfspace; hence, $\underline{a}_2^- = 0$. For

a given incident field amplitude $e_1^+(\underline{\rho})$, we define transmission and reflection coefficients as

$$\tau(\underline{a}_1^+) := \frac{\|S_{21} \cdot \underline{a}_1^+\|_2^2}{\|\underline{a}_1^+\|_2^2}, \quad (3)$$

and

$$\gamma(\underline{a}_1^+) := \frac{\|S_{11} \cdot \underline{a}_1^+\|_2^2}{\|\underline{a}_1^+\|_2^2}, \quad (4)$$

respectively. We denote the transmission coefficient of a normally incident wavefront by $\tau_{\text{normal}} = \tau\left(\begin{bmatrix} 0 & \cdots & 0 & 1 & 0 & \cdots & 0 \end{bmatrix}^T\right)$.

3. Problem formulation

We define the phase-vector of the modal coefficient vector \underline{a}_1^+ , as

$$\underline{\angle a}_1^+ = \left[\underline{\angle a}_{1,-N}^+ \quad \cdots \quad \underline{\angle a}_{1,0}^+ \quad \cdots \quad \underline{\angle a}_{1,N}^+ \right]^T,$$

where for $n = -N, \dots, N$, $a_{1,n}^+ = |a_{1,n}^+| \exp(j \underline{\angle a}_{1,n}^+)$ and $|a_{1,n}^+|$ and $\underline{\angle a}_{1,n}^+$ denote the magnitude and phase of $a_{1,n}^+$, respectively. Let P_1^M denote unit-norm vectors of the form

$$\underline{p}(\underline{\theta}) = \sqrt{\frac{1}{M}} \left[e^{j\theta_{-N}} \quad \cdots \quad e^{j\theta_0} \quad \cdots \quad e^{j\theta_N} \right]^T, \quad (5)$$

where $\underline{\theta} = \left[\theta_{-N} \quad \cdots \quad \theta_0 \quad \cdots \quad \theta_N \right]^T$ is a $M \times 1$ vector of phases where $M := 2N + 1$. Then, the problem of designing a phase-only modulated incident wavefront that maximizes the transmitted power can be stated as

$$\underline{a}_{\text{opt}} = \arg \max_{\underline{a}_1^+ \in P_1^M} \tau(\underline{a}_1^+) = \arg \max_{\underline{a}_1^+ \in P_1^M} \|S_{21} \cdot \underline{a}_1^+\|_2^2. \quad (6)$$

In the lossless setting, the scattering matrix S in Eq. (2) will be unitary, i.e., $S^H \cdot S = I$, where I is the identity matrix. Consequently, we have that

$$S_{11}^H \cdot S_{11} + S_{21}^H \cdot S_{21} = I, \quad (7)$$

so that the $\|S_{21} \cdot \underline{a}_1^+\|_2 = \sqrt{1 - \|S_{11} \cdot \underline{a}_1^+\|_2^2}$ and the optimization problem in Eq. (6) can be reformulated as

$$\underline{a}_{\text{opt}} = \arg \min_{\underline{a}_1^+ \in P_1^M} \|S_{11} \cdot \underline{a}_1^+\|_2 = \arg \min_{\underline{a}_1^+ \in P_1^M} \gamma(\underline{a}_1^+). \quad (8)$$

Thus the phase-only modulated wavefront that maximizes transmission will also minimize backscatter. The feasible set in Eq. (8) is non-convex since for $\theta_1 \neq \theta_2$ and $\alpha \in (0, 1)$, $\alpha \underline{p}(\theta_1) + (1 - \alpha) \underline{p}(\theta_2) \notin P_1^M$. Moreover, it is known [35] that Eq. (8) does not admit a closed-form solution for $\underline{a}_{\text{opt}}$ (and hence $\underline{\theta}_{\text{opt}}$). Thus we turn our attention to computational methods for solving Eq. (8).

4. Non-iterative, phase-only modulating algorithms for transmission maximization

We first consider algorithms for increasing transmission by backscatter minimization using phase-only modulated wavefronts that utilize measurements of the reflection matrix S_{11} . We assume that this matrix can be measured using the experimental techniques described in [19,20,29,31] by, in essence, transmitting $K > M$ incident wavefronts $\{\underline{a}_{1,i}^+\}_{i=1}^K$, measuring the (modal decomposition of the) backscattered wavefronts $\{\underline{a}_{1,i}^-\}_{i=1}^K$ and estimating S_{11} by solving the system of equations $\{\underline{a}_{1,i}^- = S_{11} \cdot \underline{a}_{1,i}^+\}_{i=1}^K$. We note that, even if the S_{11} matrix has been measured perfectly, the optimization problem in Eq. (8) is computationally intractable and known to be NP-hard [46, Proposition 3.3], [23]. We can make the problem computationally tractable by relaxing the phase-only constraint in Eq. (8) and allowing the elements of \underline{a}_1^+ to take on arbitrary amplitudes and phases while imposing the power constraint $\|\underline{a}_1^+\|^2 = 1$. This yields the optimization problem

$$\underline{a}_{\text{svd}} = \arg \min_{\|\underline{a}_1^+\|_2=1} \|S_{11} \cdot \underline{a}_1^+\|_2^2, \quad (9)$$

where we have relaxed the difficult constraint $\underline{a}_1^+ \in P_1^M$ into the spherical constraint $\|\underline{a}_1^+\|_2 = 1$. The problem in Eq. (9) can be solved exactly as described next.

Let $S_{21} = \sum_{i=1}^M \sigma_i \underline{u}_i \cdot \underline{v}_i^H$ and $S_{11} = \sum_{i=1}^M \tilde{\sigma}_i \tilde{\underline{u}}_i \cdot \tilde{\underline{v}}_i^H$ denote the singular value decompositions (SVD) of S_{21} and S_{11} , respectively. Here σ_i (resp. $\tilde{\sigma}_i$) is the singular value associated with the left and right singular vectors \underline{u}_i and \underline{v}_i (resp. $\tilde{\underline{u}}_i$ and $\tilde{\underline{v}}_i$), respectively. By convention, the singular values are arranged so that $\sigma_1 \geq \dots \geq \sigma_M$ and $\tilde{\sigma}_1 \geq \dots \geq \tilde{\sigma}_M$ and H denotes the complex conjugate transpose. The solution to Eq. (9) can be expressed in terms of the right singular vectors of S_{11} and S_{21} as

$$\underline{a}_{\text{svd}} = \tilde{\underline{v}}_M = \underline{v}_1. \quad (10)$$

In Eq. (10), we have employed the well-known variational characterization [14, Theorem 7.3.10] of the smallest right singular vector for the first equality and the identity $\underline{v}_i = \tilde{\underline{v}}_{M-i+1}$ derived from Eq. (7) for the second equality. This is an exact solution to the relaxed backscatter minimization problem in Eq. (9).

To get an approximation of the solution to the original unrelaxed problem in Eq. (8) we construct a wavefront as

$$\underline{a}_{\text{opt,svd}} = \underline{p}(\angle \underline{a}_{\text{svd}}). \quad (11)$$

The spherical relaxation that yields the optimization problem in Eq. (9) includes all the phase-only wavefronts in the original problem, but also includes many other wavefronts as well. We now consider a ‘tighter’ semidefinite programming (SDP) relaxation that includes

all the phase-only wavefronts in the original problem but fewer other wavefronts than the spherical relaxation does.

We note that SDP relaxations to computationally intractable problems such as Eq. (8) have gained in popularity in recent decades because there are many problems in the literature for which the SDP relaxation is known to provide a constant relative accuracy estimate for the exact solution to the unrelaxed problem [11, 26, 27]. We shall provide a similar constant relative accuracy estimate for our problem shortly in Eq. (17).

We begin by examining the objective function on the right hand side of Eq. (9). Note that

$$\|S_{11} \cdot \underline{a}_1^+\|_2^2 = ((\underline{a}_1^+)^H \cdot S_{11}^H \cdot S_{11} \cdot \underline{a}_1^+) = \text{Tr} (S_{11}^H \cdot S_{11} \cdot \underline{a}_1^+ \cdot (\underline{a}_1^+)^H), \quad (12)$$

where $\text{Tr}(\cdot)$ denotes the trace of its matrix argument. Let us define a new matrix-valued variable $A = \underline{a}_1^+ \cdot (\underline{a}_1^+)^H$. We note that A is a Hermitian, positive semi-definite matrix with rank 1 and $A_{ii} = 1/M$ whenever $\underline{a}_1^+ \in P_1^M$, where A_{ii} denotes the i th diagonal element of the matrix A . Consequently, from Eq. (12), we can derive the modified optimization problem

$$\begin{aligned} A_{\text{opt}} = \arg \min_{A \in \mathbb{C}^{M \times M}} \text{Tr} (S_{11}^H \cdot S_{11} \cdot A) \\ \text{subject to } A = A^H, A \succeq 0, \text{rank}(A) = 1 \text{ and } A_{ii} = 1/M \text{ for } i = 1, \dots, M, \end{aligned} \quad (13)$$

where the conditions $A = A^H$ and $A \succeq 0$ imply that A is a Hermitian, positive semi-definite matrix. If we can solve Eq. (13) exactly, then by construction, since A_{opt} is rank 1, we must have that $A_{\text{opt}} = \underline{a}_{\text{opt,eig}} \cdot \underline{a}_{\text{opt,eig}}^H$ with $\underline{a}_{\text{opt,eig}} \in P_1^M$ so we would have solved Eq. (8) exactly. Note that the set of rank one matrices is non-convex since the sum of two rank one matrices is not necessarily rank one. Thus the rank constraint in Eq. (13) makes the problem difficult to solve [23] even though the objective function and other constraints are convex in A .

Eliminating the difficult rank constraint yields the semi-definite programming (SDP) problem [42]

$$\begin{aligned} A_{\text{sdp}} = \arg \min_{A \in \mathbb{C}^{M \times M}} \text{Tr} (S_{11}^H \cdot S_{11} \cdot A) \\ \text{subject to } A = A^H, A \succeq 0, \text{ and } A_{ii} = 1/M \text{ for } i = 1, \dots, M, \end{aligned} \quad (14)$$

which can be efficiently solved in polynomial-time [23] using off-the shelf solvers such as CVX [13, 15] or SDPT3 [38]. See Appendix A for details.

The computational cost of solving Eq. (14) and obtaining A_{sdp} is $O(M^{4.5})$ [23] while the computational cost for obtaining $\underline{a}_{\text{opt,svd}}$ using the Lanczos method for computing only the leading singular vector is $O(M^2)$ [12]. Thus when $M > 1000$, there is a significant extra computational burden in obtaining the SDP solution. Hence, the question of when the extra computational burden of solving the SDP relaxation yields ‘large enough’ gains relative

to the spherical relaxation is of interest. We provide an answer using extensive numerical simulations in Section 7.

We note that A_{sdp} is the solution to the relaxed backscatter minimization problem in Eq. (14). If A_{sdp} thus obtained has rank 1 then we will have solved the original unrelaxed problem in Eq. (8) exactly as well. Typically, however, the matrix A_{sdp} will not be rank one so we describe a procedure next for obtaining an approximation to the original unrelaxed problem in Eq. (8).

Let $A_{\text{sdp}} = \sum_{i=1}^M \lambda_i \underline{u}_{i,\text{sdp}} \cdot \underline{u}_{i,\text{sdp}}^H$ denote the eigenvalue decomposition of A_{sdp} with the eigenvalues arranged so that $\lambda_1 \geq \dots \lambda_M \geq 0$. From A_{sdp} , we can construct a phase modulated wavefront as

$$\underline{a}_{\text{opt,sdp}} = \underline{p} \left(\underline{\angle} \underline{u}_{1,\text{sdp}} \right). \quad (15)$$

Since the SDP relaxation is a tighter relaxation than the spherical relaxation [23], we expect $\underline{a}_{\text{opt,sdp}}$ to result in higher transmission than $\underline{a}_{\text{opt,svd}}$. Note that $\underline{a}_{\text{opt,sdp}}$ given by Eq. (15) is an approximation to the solution of Eq. (8). It is not guaranteed to be the phase-only modulated wavefront that yields the highest transmission. It does however provide a lower bound on the amount of transmission that can be achieved.

In Eq. (15) we constructed a deterministic approximation to $\underline{a}_{\text{opt}}$ from A_{sdp} . Consider the randomized approximation $\tilde{\underline{a}}_{\text{opt,sdp}}$ produced from A_{sdp} as

$$\tilde{\underline{a}}_{\text{opt,sdp}} = \underline{p} \left(\underline{\angle} \left(\sum_{i=1}^M \sqrt{\lambda_i} \underline{u}_{i,\text{sdp}} \cdot \underline{u}_{i,\text{sdp}}^H \right) \cdot z \right), \quad (16)$$

where $z = z_R + \sqrt{-1} z_I$ and z_R and z_I are $M \times 1$ i.i.d. random vectors that are normally distributed with mean zero and covariance $I_M/2$. From the results of Zhang and Huang [46, Section 3.2] and So et al. [36, Corollary 1] it follows that in the lossless setting, due to the equivalence between Eq. (6) and Eq. (8), we have that

$$\frac{\pi}{4} \tau(\underline{a}_{\text{opt}}) \leq \mathbb{E}_z[\tau(\tilde{\underline{a}}_{\text{opt,sdp}})] \leq \tau(\underline{a}_{\text{opt}}) \leq 1. \quad (17)$$

In other words, the wavefront $\tilde{\underline{a}}_{\text{opt,sdp}}$ is guaranteed to produce, on average, at least 78.54% of the transmission that the optimal (unknown) wavefront $\underline{a}_{\text{opt}}$ would produce. Eq. (17) quantifies the extent to which $\tilde{\underline{a}}_{\text{opt,sdp}}$ is suboptimal to $\underline{a}_{\text{opt}}$. It provides no guarantee that the phase-only modulated wavefronts will be highly transmitting. We now provide a theoretical analysis of the transmitted power we can expect to achieve using these phase-only modulated wavefronts that will show that on average we can indeed expect them to be highly transmitting.

5. Theoretical limit of phase-only modulated light transmission

When the wavefront $\underline{a}_{\text{svd}}$ is excited, the optimal transmitted power is $\tau_{\text{opt}} := \tau(\underline{a}_{\text{svd}}) = \sigma_1^2$. Similarly, when the wavefront associated with the i -th right singular vector \underline{v}_i is transmitted,

the transmitted power is $\tau(\underline{v}_i) = \sigma_i^2$, which we refer to as the transmission coefficient of the i -th eigen-wavefront of S_{21} .

The theoretical distribution [2,3,8,25,28] of the transmission coefficients for lossless random media (referred to as the DMPK distribution) has density given by

$$f(\tau) = \lim_{M \rightarrow \infty} \frac{1}{M} \sum_{i=1}^M \delta(\tau - \tau(\underline{v}_i)) = \frac{l}{2L} \frac{1}{\tau \sqrt{1 - \tau}}, \quad \text{for } 4 \exp(-L/2l) \lesssim \tau \leq 1. \quad (18)$$

In Eq. (18), l is the mean-free path through the medium. This implies that in the regime where the DMPK distribution is valid, we expect $\tau(\underline{a}_{\text{svd}}) \approx 1$ so that (near) perfect transmission is possible using amplitude and phase modulation. We now analyze the theoretical limit of phase-only modulation in the setting where the S_{21} (or S_{11}) matrix has been measured and we have computed $\underline{a}_{\text{opt,svd}}$ or $\underline{a}_{\text{opt,sdp}}$ as in Eq. (11) and Eq. (15), respectively. In what follows, we provide a lower bound on the transmission we expect to achieve in the regime where the DMPK distribution is valid.

We begin by considering the wavefront $\underline{a}_{\text{opt,svd}}$ which yields a transmitted power given by

$$\tau(\underline{a}_{\text{opt,svd}}) = \tau(\underline{p}(\underline{a}_{\text{svd}})) = \|S_{21} \cdot \underline{p}(\underline{a}_{\text{svd}})\|_2^2 \quad (19)$$

$$= \|U \cdot \Sigma \cdot V^H \cdot \underline{p}(\underline{a}_{\text{svd}})\|_2^2 = \|\Sigma \cdot V^H \cdot \underline{p}(\underline{a}_{\text{svd}})\|_2^2, \quad (20)$$

where we arrive at the last equality by exploiting the fact that $\|U \cdot x\|_2 = \|x\|_2$ for any unitary U . Define $\tilde{\underline{p}}(\underline{a}_{\text{svd}}) = V^H \cdot \underline{p}(\underline{a}_{\text{svd}})$. Then from Eq. (20), we have that

$$\tau(\underline{a}_{\text{opt,svd}}) = \|\Sigma \cdot \tilde{\underline{p}}(\underline{a}_{\text{svd}})\|_2^2 \quad (21)$$

$$= \sum_{i=1}^M \sigma_i^2 |\tilde{p}_i(\underline{a}_{\text{svd}})|^2 \geq \sigma_1^2 |\tilde{p}_1(\underline{a}_{\text{svd}})|^2. \quad (22)$$

In the DMPK regime, we have that $\sigma_1^2 \approx 1$ from which we can deduce that

$$\tau(\underline{a}_{\text{opt,svd}}) \gtrsim |\tilde{p}_1(\underline{a}_{\text{svd}})|^2. \quad (23)$$

From Eq. (10), we have that $\underline{a}_{\text{svd}} = \underline{v}_1 = \tilde{\underline{v}}_M$ so that if

$$\underline{v}_1^H = \left[|v_{1,1}| e^{-j\angle v_{1,1}} \quad \dots \quad |v_{1,M}| e^{-j\angle v_{1,M}} \right],$$

then

$$\tilde{p}_1(\underline{a}_{\text{svd}}) = \underline{v}_1^H \cdot \underline{p}(\underline{v}_1) = \frac{1}{\sqrt{M}} \sum_{i=1}^M |v_{1,i}|, \quad (24)$$

and

$$|\tilde{p}_1(\underline{a}_{\text{svd}})|^2 = \frac{1}{M} \sum_{i=1}^M |v_{1,i}|^2 + \frac{2}{M} \sum_{i < j} |v_{1,i}| \cdot |v_{1,j}|. \quad (25)$$

Taking expectations on both sides of Eq. (25) gives us

$$\mathbb{E}[|\tilde{p}_1(\underline{a}_{\text{svd}})|^2] = \frac{1}{M} \sum_{i=1}^M \mathbb{E}[|v_{1,i}|^2] + \frac{2}{M} \sum_{i<j} \mathbb{E}[|v_{1,i}| \cdot |v_{1,j}|]. \quad (26)$$

We now invoke the maximum-entropy principle as in Pendry et al's derivations [2, 28] and assume that the vector \underline{v}_1 is uniformly distributed on the unit hypersphere. Since the uniform distribution is symmetric, for any indices i and j , we have that $\mathbb{E}[|v_{1,i}|^2] = \mathbb{E}[|v_{1,1}|^2]$ and $\mathbb{E}[|v_{1,i}| \cdot |v_{1,j}|] = \mathbb{E}[|v_{1,1}| \cdot |v_{1,2}|]$. Consequently Eq. (26) simplifies to

$$\mathbb{E}[|\tilde{p}_1(\underline{a}_{\text{svd}})|^2] = \mathbb{E}[|v_{1,1}|^2] + \frac{2M(M-1)}{2M} \mathbb{E}[|v_{1,1}| \cdot |v_{1,2}|] \quad (27)$$

Since $\|\underline{v}_1\|_2^2 = \sum_{i=1}^M |v_{1,i}|^2 = 1$, from symmetry considerations, we have that

$$\mathbb{E}[|v_{1,1}|^2] = \frac{1}{M}. \quad (28)$$

Substituting Eq. (28) into Eq. (27) gives

$$\mathbb{E}[|\tilde{p}_1(\underline{a}_{\text{svd}})|^2] = (M-1) \mathbb{E}[|v_{1,1}| \cdot |v_{1,2}|] + \frac{1}{M}. \quad (29)$$

A useful fact that will facilitate analytical progress is that the distribution of the complex-valued random variables $v_{1,i}$ can be exactly characterized. Specifically, we have that [30, Chap. 3a]

$$v_{1,i} \stackrel{d}{=} \frac{g_i}{\sqrt{|g_1|^2 + \dots + |g_M|^2}}, \quad (30)$$

where $\stackrel{d}{=}$ denotes equality in distribution and $g_i = x_i + \sqrt{-1} y_i$ and x_i and y_i are i.i.d. normally distributed variables with mean zero and variance 1. Let $r_i = |g_i|$. The random variables $|r_i|$ are i.i.d. Rayleigh distributed [32] with density given by

$$f_{r_i}(r) = r e^{-\frac{r^2}{2}} \quad \text{for } r \geq 0.$$

The random variable $s_3 := \sqrt{\sum_{i=3}^M r_i^2}$, by construction, is independent of r_1 and r_2 and is χ distributed with $2(M-2)$ degrees of freedom. It has density given by [10, Section 11.3]

$$f_{s_3}(r) = \frac{2^{3-M} \cdot r^{2M-5} e^{-\frac{r^2}{2}}}{\Gamma(M-2)} \quad \text{for } r \geq 0.$$

The first term on the right hand side of Eq. (29) can be expressed in terms of these intermediate variables as

$$\begin{aligned} \mathbb{E}[|v_{1,1}| \cdot |v_{1,2}|] &= \mathbb{E}\left[\frac{|g_1| \cdot |g_2|}{|g_1|^2 + |g_2|^2 + (|g_3|^2 + \dots + |g_M|^2)}\right] = \mathbb{E}\left[\frac{r_1 \cdot r_2}{r_1^2 + r_2^2 + s_3^2}\right] \\ &= \int_0^\infty \int_0^\infty \int_0^\infty \frac{r_1 \cdot r_2}{r_1^2 + r_2^2 + s_3^2} r_1 e^{-\frac{r_1^2}{2}} \cdot r_2 e^{-\frac{r_2^2}{2}} \cdot \frac{2^{3-M} \cdot s_3^{2M-5} e^{-\frac{s_3^2}{2}}}{\Gamma(M-2)} dr_1 dr_2 ds_3 \\ &= \frac{2^{3-M}}{\Gamma(M-2)} \int_0^\infty \int_0^\infty \int_0^\infty \frac{r_1^2 \cdot r_2^2 \cdot s_3^{2M-5}}{r_1^2 + r_2^2 + s_3^2} e^{-\frac{r_1^2+r_2^2+s_3^2}{2}} dr_1 dr_2 ds_3. \end{aligned}$$

Let $r_1 = r \sin(t) \cos(p)$, $r_2 = r \sin(t) \sin(p)$ and $s_3 = r \cos(t)$. With these change of variables we have that

$$\begin{aligned} \mathbb{E}[|v_{1,1}| \cdot |v_{1,2}|] &= \frac{2^{3-M}}{\Gamma(M-2)} \times \\ &\int_0^{\frac{\pi}{2}} \int_0^{\frac{\pi}{2}} \int_0^\infty \frac{\cos^2(p) (r \cos(t))^{2M} \sec(t) \sin^2(p) \tan^4(t)}{r^3} e^{-\frac{r^2}{2}} dr dt dp \quad (31) \\ &= \frac{\pi}{4M}. \end{aligned}$$

Substituting Eq. (31) into Eq.(29) gives us

$$\mathbb{E}[|\tilde{p}_1(\underline{a}_{\text{svd}})|^2] = \frac{\pi}{4} + \frac{4-\pi}{4M}. \quad (32)$$

Taking expectations on both sides of Eq. (23) and substituting Eq. (32) into the right hand side yields the inequality

$$\mathbb{E}[\tau(\underline{a}_{\text{opt,svd}})] \gtrsim \frac{\pi}{4} + \frac{4-\pi}{4M}. \quad (33)$$

Since $\tau(\underline{a}_{\text{opt,sdp}}) \geq \tau(\underline{a}_{\text{opt,svd}})$, Eq. (33) yields the inequality

$$\mathbb{E}[\tau(\underline{a}_{\text{opt,sdp}})] \geq \mathbb{E}[\tau(\underline{a}_{\text{opt,svd}})] \gtrsim \frac{\pi}{4} + \frac{4-\pi}{4M}. \quad (34)$$

Letting $M \rightarrow \infty$ on both sides on Eq. (34) gives us

$$\lim_{M \rightarrow \infty} \mathbb{E}[\tau(\underline{a}_{\text{opt,sdp}})] \geq \lim_{M \rightarrow \infty} \mathbb{E}[\tau(\underline{a}_{\text{opt,svd}})] \gtrsim \frac{\pi}{4}. \quad (35)$$

From Eq. (35) we expect to achieve at least 25 $\pi\%$ when the S_{21} (or S_{11}) matrix has been measured and we compute the phase-only modulated wavefront using $\underline{a}_{\text{opt,svd}}$ or $\underline{a}_{\text{opt,sdp}}$. In contrast, amplitude and phase modulation yields (nearly) 100% transmission; thus the phase-only modulation incurs an average loss of at most 22%.

We now show that when M is large and we are in the DMPK regime, with very high probability, we can expect to lose not much more than 22% of the transmitted power relative to an amplitude and phase modulated wavefront. To that end we note that by the triangle inequality

$$\sum_{i=1}^M |x_i + \delta_i| - \sum_{i=1}^M |x_i| \leq 1 \cdot \sum_{i=1}^M |\delta_i|.$$

This implies that $\sqrt{M} \tilde{p}_1(\cdot)$ is a 1-Lipschitz function of the argument. Under the assumption that $\underline{a}_{\text{svd}} = \underline{v}_1$ has uniform distribution on the unit hypersphere, from the results in [22, Theorem 2.3 and Prop. 1.8] it follows that there are positive constants c and C such that for M large enough, and for all $\epsilon > 0$

$$\mathbb{P}\left(\sqrt{M} |\tilde{p}_1(\underline{a}_{\text{svd}}) - \mathbb{E}[\tilde{p}_1(\underline{a}_{\text{svd}})]| \geq \epsilon\right) \leq C e^{(-cM\epsilon^2)} \quad (36)$$

or equivalently, by setting $\epsilon \mapsto \sqrt{M}\epsilon$, that

$$\mathbb{P}(|\tilde{p}_1(\underline{a}_{\text{svd}}) - \mathbb{E}[\tilde{p}_1(\underline{a}_{\text{svd}})]| \geq \epsilon) \leq C e^{(-cM^2\epsilon^2)}. \quad (37)$$

Eq. (37) shows that we expect $|\tilde{p}_1(\underline{a}_{\text{svd}})|$ and hence $|\tilde{p}_1(\underline{a}_{\text{svd}})|^2$ to be concentrated around its mean given by Eq. (32). Thus, from Eq. (23) we can conclude that as $M \rightarrow \infty$ we expect to transmit very close to 25% with very high probability.

6. Iterative, phase-only modulated algorithms for transmission maximization

In Section 4 we described three non-iterative techniques for constructing approximations to $\underline{a}_{\text{opt}}$ in Eq. (8) via backscatter analysis that first require the S_{11} to be measured and then compute $\underline{a}_{\text{opt,svd}}$, $\underline{a}_{\text{opt,sdp}}$ or $\tilde{\underline{a}}_{\text{opt,sdp}}$ using Eq. (11), Eq. (15) and Eq. (16), respectively.

We now develop physically-realizable, iterative algorithms for increasing transmission by backscatter minimization that utilize significantly fewer measurements than the $O(M)$ measurements it would take to first estimate S_{11} and subsequently construct $\underline{a}_{\text{opt,svd}}$ or $\underline{a}_{\text{opt,sdp}}$. We note we do yet not have an theoretical guarantees that these iterative algorithms will indeed converge rapidly and produce highly transmitting wavefronts. We provide evidence, in Section 7, of their rapid convergence using results from numerical simulations.

6.A. Steepest Descent Method

We first consider an iterative method, based on the method of steepest descent, for finding the wavefront \underline{a}_1^+ that minimizes the objective function $\|S_{11} \cdot \underline{a}_1^+\|_2^2$. At this stage, we consider arbitrary vectors \underline{a}_1^+ instead of phase-only modulated vectors $\underline{a}_1^+ \in P_1^M$. The algorithm utilizes the negative gradient of the objective function to update the incident wavefront as

$$\tilde{\underline{a}}_{1,(k)}^+ = \underline{a}_{1,(k)}^+ - \mu \left. \frac{\partial \|S_{11} \cdot \underline{a}_1^+\|_2^2}{\partial \underline{a}_1^+} \right|_{\underline{a}_1^+ = \underline{a}_{1,(k)}^+} \quad (38)$$

$$= \underline{a}_{1,(k)}^+ - 2\mu S_{11}^H \cdot S_{11} \cdot \underline{a}_{1,(k)}^+, \quad (39)$$

where $\underline{a}_{1,(k)}^+$ represents the modal coefficient vector of the incident wavefront produced at the k -th iteration of the algorithm and μ is a positive stepsize. If we renormalize $\tilde{\underline{a}}_{1,(k)}^+$ to have $\|\tilde{\underline{a}}_{1,(k)}^+\|_2 = 1$, we obtain the iteration

$$\underline{a}_{1,(k+1)}^+ = \frac{(I - 2\mu S_{11}^H \cdot S_{11}) \cdot \underline{a}_{1,(k)}^+}{\|(I - 2\mu S_{11}^H \cdot S_{11}) \cdot \underline{a}_{1,(k)}^+\|_2}. \quad (40)$$

Eq. (40) is precisely the power iteration [39, Algorithm 27.1] on the matrix $(I - 2\mu S_{11}^H \cdot S_{11})$. Thus [39, Theorem 27.1], in the limit of $k \rightarrow \infty$, the incident wavefront $\underline{a}_{1,(k+1)}^+$ will converge to $\underline{a}_{\text{svd}}$, which is the largest eigenvector of $(I - 2\mu S_{11}^H \cdot S_{11})$ provided $\tilde{\sigma}_1 > \tilde{\sigma}_2$ and we select

Algorithm 1 Steepest descent algorithm for finding $\underline{a}_{\text{svd}}$

- 1: Input: $\underline{a}_{1,(0)}^+$ = Initial random vector with unit norm
 - 2: Input: $0 < \mu < 1/(\tilde{\sigma}_1^2 + \tilde{\sigma}_M^2)$ = step size
 - 3: Input: ϵ = Termination condition
 - 4: $k = 0$
 - 5: **while** $\|S_{11} \cdot \underline{a}_{1,(k)}^+\|_2^2 > \epsilon$ **do**
 - 6: $\tilde{\underline{a}}_{1,(k)}^+ = \underline{a}_{1,(k)}^+ - 2\mu S_{11}^H \cdot S_{11} \cdot \underline{a}_{1,(k)}^+$
 - 7: $\underline{a}_{1,(k+1)}^+ = \tilde{\underline{a}}_{1,(k)}^+ / \|\tilde{\underline{a}}_{1,(k)}^+\|_2$
 - 8: $k = k + 1$
 - 9: **end while**
-

$\mu < 1/(\tilde{\sigma}_1^2 + \tilde{\sigma}_M^2)$. In the DMPK regime, $\tilde{\sigma}_M^2 = 1 - \sigma_1^2 \approx 0$ while $\tilde{\sigma}_1^2 = 1 - \sigma_M^2 \approx 1$. Thus selecting $\mu \lesssim 1$ is justified. This iteration forms the basis for Algorithm 1 which produces a highly transmitting wavefront by iterative refinement the wavefront $\underline{a}_{1,(k+1)}^+$.

We now describe how the update equation given by Eq. (39), which requires computation of the gradient $S_{11}^H \cdot S_{11} \cdot \underline{a}_{1,(k)}^+$, can be physically implemented even though we have not measured S_{11} a priori.

Let $\text{flipud}(\cdot)$ represent the operation of flipping a vector or a matrix argument upside down so that the first row becomes the last row and so on. Let $F = \text{flipud}(I)$ where I is the identity matrix, and let $*$ denote complex conjugation. In our previous work [18], we showed that reciprocity of the scattering system implies that

$$S_{11}^H = F \cdot S_{11}^* \cdot F, \quad (41)$$

which can be exploited to make the gradient vector $S_{11}^H \cdot S_{11} \cdot \underline{a}_{1,(k)}^+$ physically measurable. To that end, we note that Eq. (41) implies that

$$S_{11}^H \cdot \underline{a}_1^- = F \cdot S_{11}^* \cdot F \cdot \underline{a}_1^- = F \cdot (S_{11} \cdot (F \cdot (\underline{a}_1^-)^*))^*. \quad (42)$$

where $\underline{a}_1^- = S_{11} \cdot \underline{a}_{1,(k)}^+$. Thus, we can physically measure $S_{11}^H \cdot S_{11} \cdot \underline{a}_{1,(k)}^+$, by performing the following sequence of operations and the accompanying measurements:

1. Transmit $\underline{a}_{1,(k)}^+$ and measure the backscattered wavefront $\underline{a}_1^- = S_{11} \cdot \underline{a}_{1,(k)}^+$.
2. Transmit the wavefront obtained by time-reversing the wavefront whose modal coefficient vector is \underline{a}_1^- or equivalently transmitting the wavefront $F \cdot (\underline{a}_1^-)^*$.
3. Measure the resulting backscattered wavefront corresponding to $S_{11} \cdot (F \cdot (\underline{a}_1^-)^*)$ and time-reverse it to yield the desired gradient vector $S_{11}^H \cdot S_{11} \cdot \underline{a}_{1,(k)}^+$ as shown in Eq. (42).

The above represents a physically realizable scheme for measuring the gradient vector, which we proposed in our previous paper [18]. Since time-reversal can be implemented using phase-conjugating mirror, we referred to this as the *double phase-conjugating method*.

For the setting considered here, we have the additional physically-motivated restriction that all transmitted wavefronts $\underline{a}_1^+ \in P_1^M$. However, the wavefront \underline{a}_1^- can have arbitrary amplitudes and so will the wavefront obtained by time-reversing it (as in Step 2 above) thereby violating the phase-only modulating restriction and making Algorithm 1, physically unrealizable. This is also why algorithms of the sort considered by others in array processing e.g. [35] cannot be directly applied here.

This implies that even though Algorithm 1 provably converges to $\underline{a}_{\text{svd}}$, it cannot be used to compute $\underline{a}_{\text{opt,svd}}$ as in Eq. (11) because it is not physically implementable given the phase-only modulation constraint. To mitigate this problem, we propose modifying the update step in Eq. (39) to

$$\tilde{\underline{a}}_{1,(k)}^+ = \underline{p} \left(\underline{a}_{1,(k)}^+ - 2\mu\bar{a} S_{11}^H \cdot \underline{p}(\underline{S}_{11} \cdot \underline{a}_{1,(k)}^+) \right), \quad (43)$$

where \bar{a} is chosen such that all magnitudes of modal coefficients of $\bar{a}\underline{p}(\underline{a}_1^-)$ are set to the average magnitude of modal coefficients of \underline{a}_1^- . Then, by applying Eq. (41) as before, we can physically measure $\bar{a} S_{11}^H \cdot \underline{p}(\underline{S}_{11} \cdot \underline{a}_{1,(k)}^+)$ by performing the following sequence of operations and the accompanying measurements:

1. Transmit $\underline{a}_{1,(k)}^+$ and measure the backscattered wavefront $\underline{a}_1^- = S_{11} \cdot \underline{a}_{1,(k)}^+$.
2. Compute the scalar $\bar{a} = \frac{\sum_{n=-N}^N |a_{1,n}^-|}{\sqrt{M}}$.
3. Transmit the (phase-only modulated) wavefront obtained by time-reversing the wavefront whose modal coefficient vector is $\underline{p}(\underline{a}_1^-)$.
4. Measure the resulting backscattered wavefront, time-reverse it, and scale it with \bar{a} to yield the desired gradient vector.

This modified iteration in Eq. (43) leads to the algorithm in the left column of Table 1 and its physical counterpart in the right column of Table 1. We do not have a convergence theory for this algorithm; we propose selecting $\mu < 1$ as before.

6.B. Gradient Method

The wavefront updating step for the algorithm described in Table 1 first updates both the amplitude and phase of the incident wavefront (in Step 7) and then ‘projects it’ onto the set of phase-only modulated wavefronts (in Step 8). We now develop a gradient-based method that only updates the phase of the incident wavefront. From Eq. (8), the objective function of interest is $\|S_{11} \cdot \underline{p}(\underline{\theta})\|_2^2$ which depends on the phase-only modulated wavefront. The algorithm

Vector Operation	Physical Operation
1 : $\underline{a}_1^- = S_{11} \cdot \underline{a}_{1,(k)}^+$	1 : $\underline{a}_{1,(k)}^+ \xrightarrow{\text{Backscatter}} \underline{a}_1^-$
2 : $\bar{a} = \frac{\sum_{n=-N}^N a_{1,n}^- }{\sqrt{M}}$	2 : $\bar{a} = \frac{\sum_{n=-N}^N a_{1,n}^- }{\sqrt{M}}$
3 : $\underline{a}_1^- \leftarrow \underline{p}(\underline{a}_1^-)$	3 : $\underline{a}_1^- \leftarrow \underline{p}(\underline{a}_1^-)$
4 : $\underline{a}_1^+ = F \cdot (\underline{a}_1^-)^*$	4 : $\underline{a}_1^- \xrightarrow{\text{PCM}} \underline{a}_1^+$
5 : $\underline{a}_1^- = S_{11} \cdot \underline{a}_1^+$	5 : $\underline{a}_1^+ \xrightarrow{\text{Backscatter}} \underline{a}_1^-$
6 : $\underline{a}_1^+ = F \cdot (\underline{a}_1^-)^*$	6 : $\underline{a}_1^- \xrightarrow{\text{PCM}} \underline{a}_1^+$
7 : $\tilde{\underline{a}}_1^+ = \underline{a}_{1,(k)}^+ - 2\mu\bar{a}\underline{a}_1^+$	7 : $\tilde{\underline{a}}_1^+ = \underline{a}_{1,(k)}^+ - 2\mu\bar{a}\underline{a}_1^+$
8 : $\underline{a}_{1,(k+1)}^+ = \underline{p}(\underline{a}_1^+)$	8 : $\underline{a}_{1,(k+1)}^+ = \underline{p}(\underline{a}_1^+)$

Table 1. Steepest descent algorithm for refining a highly transmitting phase-only modulated wavefront. The first column represents vector operations. The second column represents the physical (or experimental) counterpart. The operation $\underline{a}_1^- \mapsto F \cdot (\underline{a}_1^-)^*$ can be realized via the use of a phase-conjugating mirror (PCM). The algorithm terminates when $\|\gamma(\underline{a}_{1,(k+1)}^+) - \gamma(\underline{a}_{1,(k)}^+)\|_2 < \epsilon$, where ϵ is a preset threshold.

utilizes the negative gradient of the objective function with respect to the phase vector to update the phase vector of the incident wavefront as

$$\underline{\theta}_{1,(k+1)}^+ = \underline{\theta}_{1,(k)}^+ - \sqrt{M}\mu \left. \frac{\partial \|S_{11} \cdot \underline{p}(\underline{\theta})\|_2^2}{\partial \underline{\theta}} \right|_{\underline{\theta}=\underline{\theta}_{1,(k)}^+}, \quad (44)$$

where $\underline{\theta}_{1,(k)}^+$ represents the phase vector of the wavefront produced at the k -th iteration of the algorithm and μ is a positive stepsize. In Appendix B, we show that

$$\left. \frac{\partial \|S_{11} \cdot \underline{p}(\underline{\theta})\|_2^2}{\partial \underline{\theta}} \right|_{\underline{\theta}=\underline{\theta}_{1,(k)}^+} = 2\text{Im} \left[\text{diag}\{\underline{p}(-\underline{\theta}_{1,(k)}^+)\} \cdot S_{11}^H \cdot S_{11} \cdot \underline{p}(\underline{\theta}_{1,(k)}^+) \right], \quad (45)$$

where $\text{diag}\{\underline{p}(-\underline{\theta}_{1,(k)}^+)\}$ denotes a diagonal matrix with entries $\underline{p}(-\underline{\theta}_{1,(k)}^+)$ along its diagonal. From Eq. (45), we have that

$$\begin{aligned} \left\| \frac{\partial \|S_{11} \cdot \underline{p}(\underline{\theta})\|_2^2}{\partial \underline{\theta}} \Big|_{\underline{\theta}=\underline{\theta}_{1,(k)}^+} \right\|_2 &= \left\| 2\text{Im} \left[\text{diag}\{\underline{p}(-\underline{\theta}_{1,(k)}^+)\} \cdot S_{11}^H \cdot S_{11} \cdot \underline{p}(\underline{\theta}_{1,(k)}^+) \right] \right\|_2, \\ &\leq 2\|\text{diag}\{\underline{p}(-\underline{\theta}_{1,(k)}^+)\}\|_2 \cdot \tilde{\sigma}_1^2 \leq 2\frac{1}{\sqrt{M}} \cdot 1 = \frac{2}{\sqrt{M}}. \end{aligned}$$

This motivates our separation of the \sqrt{M} factor from the stepsize in Eq. (45) since the resulting μ can be chosen to be $O(1)$ and independent of M . Substituting Eq. (45) into the right-hand side of Eq. (44) yields the iteration

$$\underline{\theta}_{1,(k+1)}^+ = \underline{\theta}_{1,(k)}^+ - 2\sqrt{M}\mu \text{Im} \left[\text{diag}\{\underline{p}(-\underline{\theta}_{1,(k)}^+)\} \cdot S_{11}^H \cdot S_{11} \cdot \underline{p}(\underline{\theta}_{1,(k)}^+) \right]. \quad (46)$$

To evaluate the update Eq. (46), it is necessary to measure the gradient vector $S_{11}^H \cdot S_{11} \cdot \underline{p}(\underline{\theta}_{1,(k)}^+)$. For the same reason as in the steepest descent scheme, we cannot use double-phase conjugation introduced in our previous paper [18] because of the phase-only modulating restriction. Therefore, we propose modifying the update step in Eq. (46) to

$$\underline{\theta}_{1,(k+1)}^+ = \underline{\theta}_{1,(k)}^+ - 2\sqrt{M}\mu \bar{a} \text{Im} \left[\text{diag}\{\underline{p}(-\underline{\theta}_{1,(k)}^+)\} \cdot S_{11}^H \cdot \underline{p}(\underline{S}_{11} \cdot \underline{p}(\underline{\theta}_{1,(k)}^+)) \right], \quad (47)$$

and we use the modified double-phase conjugation as

1. Transmit $\underline{p}(\underline{\theta}_{1,(k)}^+)$ and measure the backscattered wavefront $\underline{a}_1^- = S_{11} \cdot \underline{p}(\underline{\theta}_{1,(k)}^+)$;
2. Compute the scalar $\bar{a} = \frac{\sum_{n=-N}^N |a_{1,n}^-|}{\sqrt{M}}$;
3. Transmit the phase-only modulated wavefront obtained by time-reversing the wavefront whose modal coefficient vector is $\underline{p}(\underline{a}_1^-)$;
4. Measure the resulting backscattered wavefront, time-reverse it, and scale it with \bar{a} to yield the desired gradient vector.

The phase-updating iteration in Eq. (47) leads to the algorithm in the left column of Table 2 and its physical counterpart in the right column of Table 2. We do not have a convergence theory for this algorithm; we propose selecting the value of $\mu = O(1)$ which leads to fastest convergence by a line search.

7. Numerical simulations

To validate the proposed algorithms and the theoretical limits of phase-only wavefront optimization, we adopt the numerical simulation protocol described in [18]. Specifically, we

Vector Operation	Physical Operation
1: $\underline{a}_1^- = S_{11} \cdot \underline{p}(\underline{\theta}_{1,(k)}^+)$	1: $\underline{p}(\underline{\theta}_{1,(k)}^+) \xrightarrow{\text{Backscatter}} \underline{a}_1^-$
2: $\bar{a} = \frac{\sum_{n=-N}^N a_{1,n}^- }{\sqrt{M}}$	2: $\bar{a} = \frac{\sum_{n=-N}^N a_{1,n}^- }{\sqrt{M}}$
3: $\underline{a}_1^- \leftarrow \underline{p}(\underline{a}_1^-)$	3: $\underline{a}_1^- \leftarrow \underline{p}(\underline{a}_1^-)$
4: $\underline{a}_1^+ = F \cdot (\underline{a}_1^-)^*$	4: $\underline{a}_1^- \xrightarrow{\text{PCM}} \underline{a}_1^+$
5: $\underline{a}_1^- = S_{11} \cdot \underline{a}_1^+$	5: $\underline{a}_1^+ \xrightarrow{\text{Backscatter}} \underline{a}_1^-$
6: $\underline{a}_1^+ = F \cdot (\underline{a}_1^-)^*$	6: $\underline{a}_1^- \xrightarrow{\text{PCM}} \underline{a}_1^+$
7: $\underline{\theta}_{1,(k+1)}^+ = \underline{\theta}_{1,(k)}^+ - 2\sqrt{M}\mu\bar{a} \text{Im} \left[\text{diag}\{\underline{p}(-\underline{\theta}_{1,(k)}^+)\} \cdot \underline{a}_1^+ \right]$	

Table 2. Gradient algorithm for transmission maximization. The first column contains the updating iteration in Eq. (47) split into a series of individual updates so that they may be mapped into their physical (or experimental) counterparts in the column to their right. The operation $\underline{a}_1^- \mapsto F \cdot (\underline{a}_1^-)^*$ can be realized via the use of a phase-conjugating mirror (PCM). The algorithm terminates when $\|\gamma(\underline{p}(\underline{\theta}_{1,(k+1)}^+)) - \gamma(\underline{p}(\underline{\theta}_{1,(k)}^+))\|_2 < \epsilon$, where ϵ is a preset threshold.

compute the scattering matrices in Eq. (2) via a spectrally accurate, T-matrix inspired integral equation solver that characterizes fields scattered from each cylinder in terms of their traces expanded in series of azimuthal harmonics. As in [18], interactions between cylinders are modeled using 2D periodic Green’s functions. The method constitutes a generalization of that in [24], in that it does not force cylinders in a unit cell to reside on a line but allows them to be freely distributed throughout the cell. As in [18], all periodic Green’s functions/lattice sums are rapidly evaluated using a recursive Shank’s transform using the methods described in [33, 34]. Our method exhibits exponential convergence in the number of azimuthal harmonics used in the description of the field scattered by each cylinder. As in [18], in the numerical experiments below, care was taken to ensure 11-digit accuracy in the entries of the computed scattering matrices.

We now describe how the simulations were performed. We generated a random scattering system with $D = 197\lambda$, $r = 0.11\lambda$, $\tilde{L} = 3.4 \times 10^5\lambda$, $N_c = 430,000$, $n_d = 1.3$ and $M = 395$. The locations of the scatterers were selected randomly and produced a system with $\bar{l} = 6.69\lambda$, where \bar{l} is the average distance to the nearest scatterer. Let L denote the thickness of the

scattering system we are interested in analyzing. We vary L from λ to \tilde{L} and for each value of L we compute the scattering matrices associated with only the scatterers contained in the $(0, L)$ portion of the $(0, \tilde{L})$ system we have generated. This construction ensures that the average density per “layer” of the medium is about the same. We computed the reported statistics by simulating 1700 random realizations of the scattering system.

First we compare the transmitted power achieved by the non-iterative algorithms that utilize knowledge of the entire S_{11} matrix to compute the wavefronts $\underline{a}_{\text{opt,svd}}$, $\underline{a}_{\text{opt,sdp}}$ and $\tilde{\underline{a}}_{\text{opt,sdp}}$ given by Eq. (11), Eq. (15) and Eq. (16), respectively. Fig. 3 compares the transmitted power for the SVD and SDP based algorithms as a function of the thickness L/λ of the scattering system averaged over 1700 random realizations of the scattering system.

As expected, the wavefront $\underline{a}_{\text{opt,sdp}}$ realizes increased transmission relative to the wavefront $\underline{a}_{\text{opt,svd}}$. However, as the thickness of the medium increases, the gain vanishes. Typically $\underline{a}_{\text{opt,sdp}}$ increases transmission by about 1 – 5% relative to $\underline{a}_{\text{opt,svd}}$. The wavefront $\tilde{\underline{a}}_{\text{opt,sdp}}$ is clearly suboptimal. Fig. 3 also shows the accuracy of our theoretical prediction of $25\pi\% \approx 78.5\%$ transmission using phase-only modulation for highly backscattering (or thick) random media in the same regime where the DMPK theory predicts perfect transmission using amplitude and phase modulated wavefronts. The relatively small one-standard-deviation error bars displayed validate the prediction based on Eq. (37).

Recall that the computational cost of computing $\underline{a}_{\text{opt,sdp}}$ is $O(M^{4.5})$ while the cost for computing $\underline{a}_{\text{opt,svd}}$ is $O(M^2)$. Fig. 3 suggests that for large M , the significantly extra computational effort for computing $\underline{a}_{\text{opt,sdp}}$ might not be worth the effort for strongly scattering random media.

In Fig. 4, we plot the transmitted power achieved by undersampling the number of control modes by a factor of 4, computing the resulting S_{21} matrix, and constructing the amplitude and phase modulated eigen-wavefront associated with the largest right singular vector. This is what would happen if we were to implement the ‘superpixel’-based amplitude and phase modulation scheme described in [41] in the framework of a system with periodic boundary conditions. As can be seen, phase-only modulation yields higher transmission than amplitude and phase modulation with undersampled modes. We are presently studying whether the same result holds true in systems without periodic boundary conditions as considered in [5].

Let $\underline{a}_{\text{equal}} = \underline{p}(\begin{bmatrix} 0 & \dots & 0 & \dots & 0 \end{bmatrix})$ represent a wavefront with equal phases (set arbitrarily to zero). Fig. 4 also plots the transmitted power achieved by the wavefront $\underline{a}_{\text{equal}}$. The plot reveals that both the SVD and the SDP based algorithms realize significant gains relative to this vector¹.

We shall now illustrate the performance of the iterative methods. For the iterative methods,

¹A normally incident wavefront also yields about the same transmitted power. Note that a normally incident wavefront cannot be synthesized using phase-only modulation using the setup in Fig. 1.

let us denote the wavefront vector produced by the algorithm at the k -th iteration with stepsize μ as $\underline{a}_{1,(k)}^{+,\mu}$. In the simulations that follow, we chose the optimal μ for each algorithm, for every realization of the scattering medium, by computing

$$\mu_{\text{opt}} = \arg \max_{\mu_{\min} \leq \mu \leq \mu_{\max}} \sum_{k=0}^{50} \tau \left(\underline{a}_{1,(k)}^{+,\mu} \right). \quad (48)$$

In other words, the optimal μ was obtained by a line search, i.e., by running the algorithms over a fixed set of discretized values of μ between μ_{\min} and μ_{\max} , and choosing the μ that converged the fastest. In our experiments, we set $\mu_{\min} = 0.001$ (resp. 0.001) and $\mu_{\max} = 1$ (resp. 5) for the steepest descent (resp. gradient descent) algorithm.

Fig. 5 compares the rate of convergence of the phase-only modulated steepest descent and gradient descent based algorithms and the rate of convergence of the amplitude and phase modulated steepest descent based algorithm from [18, Algorithm 1]. Here we are in a setting with $D = 197\lambda$, $L = 3.4 \times 10^5 \lambda$, $r = 0.11\lambda$, $N_c = 430,000$ dielectric cylinders with $n_d = 1.3$, $M = 395$, $\bar{l} = 6.69\lambda$. The amplitude and phase modulated steepest descent algorithm produces a wavefront that converges to 95% of the near optimum in about 5 – 10 iterations as shown in Fig. 5. The phase-only modulated steepest descent algorithm yields a highly transmitting wavefront within 5 – 10 iterations. The phase-only modulated gradient descent algorithm also increases in transmission and converges in 15 – 20 iterations. The fast convergence properties of the steepest descent based method make it suitable for use in an experimental setting where it might be infeasible to measure the S_{11} matrix first.

Fig. 6 compares the maximum transmitted power achieved after 50 iterations as a function of thickness L/λ for the iterative, phase-only modulated steepest descent and gradient descent methods and the non-iterative SVD and SDP methods. The non-iterative methods increase transmission by 8.3% relative to the steepest descent method. The gradient descent method performs poorly relative to the steepest descent method but still achieves increased transmission relative to the non-adaptive ‘equal-phase’ wavefront.

Fig. 7 plots the average number of iterations required to reach 95% of the respective optima for the phase-only modulated steepest descent and gradient descent algorithms as a function of the thickness L/λ of the scattering system. On average the steepest descent algorithm converges in about 15 – 20 iterations while the gradient descent algorithm converges in about 35 – 45 iterations.

As the steepest descent algorithm converges faster and realizes 15 – 20% greater transmitted power, but only loses 10% transmission relative to the non-iterative phase-only modulated SVD and SDP algorithms, it is the best option for use in an experimental setting.

Since determining the optimal size μ via a line search increases the number of measurements, we now investigate the sensitivity of the phase-only steepest descent algorithm to the

choice of stepsize. Fig. 8 plots the average transmitted power as a function of the number of iterations and the stepsize μ for the steepest descent algorithm. This plot reveals that there is a broad range of μ for which the algorithm converges rapidly. Fig. 9 shows the transmitted power achieved after 50 iterations of the phase-only modulated steepest descent algorithm as a function of the stepsize μ and the thickness L/λ of the scattering system showing that there is a wide range of allowed values for μ for which the steepest descent algorithm performs well. We have experimentally found that setting $\mu \approx 0.65$ yields fast convergence about 15 – 20 iterations under a broad range of conditions.

Finally, we consider the setting where the scatterers are absorptive with a refractive index given by $n_d = 1.3 - j\kappa$. Here, backscatter minimization as a general principle for increasing transmission is clearly sub-optimal since an input with significant absorption can also minimize backscatter. In Fig. 10, we compare the gain, relative to τ_{equal} , of the transmitted power achieved by the iterative phase-only steepest descent algorithm and non-iterative algorithms that assume knowledge of the S_{21} matrix. Specifically, we compare the transmissions achieved by the wavefront produced by the backscatter analysis based steepest descent algorithm, the optimal transmission maximizing wavefront \underline{v}_1 which requires amplitude and phase modulation and the wavefront $\underline{a}_{\text{opt,sdp}}$ obtained as in Eq. (15), except with A_{sdp} defined as the solution of the optimization problem

$$A_{\text{sdp}} = \arg \max_{A \in \mathbb{C}^{M \times M}} \text{Tr} (S_{21}^H \cdot S_{21} \cdot A) \quad (49)$$

subject to $A = A^H$, $A \succeq 0$, and $A_{ii} = 1/M$ for $i = 1, \dots, M$.

Fig. 10 shows that the iterative method realizes a significant increase in transmission even when the scatterers are weakly absorptive. The iterative algorithm converges rapidly, in about as many iterations as in the lossless setting for the same range of stepsizes

8. Conclusions

We have shown theoretically and using numerically rigorous simulation that non-iterative, phase-only modulated techniques for transmission maximization using backscatter analysis can expect to achieve about $25 \pi\% \approx 78.5\%$ transmission in highly backscattering random media in the DMPK regime where amplitude and phase modulated can yield 100% transmission. We have developed two new, iterative and physically realizable algorithms for constructing highly transmitting phase-only modulated wavefronts using backscatter analysis. We showed using numerical simulations that the steepest descent variant outperforms the gradient descent variant and that the wavefront produced by the steepest descent algorithm achieves about 71% transmission while converging within 15 – 20 measurements. The development of iterative phase-only modulated algorithms that bridge the 10% transmission gap between the steepest descent algorithm presented here and the non-iterative SVD and SDP

algorithms remains an important open problem. We would also like to theoretically analyze the convergence properties of the iterative methods presented so we might better understand why the physically realizable variant of gradient descent method performs poorly compared to the physically realizable variant of the steepest descent method.

The proposed algorithms are quite general and may be applied to scattering problems beyond the 2D setup described in the simulations. A detailed study, guided by the insights in [5], of the impact of periodic boundary conditions on the results obtained is also underway.

Acknowledgements

This work was partially supported by an ONR Young Investigator Award N000141110660, an NSF grant CCF-1116115, an AFOSR Young Investigator Award FA9550-12-1-0266 and an AFOSR DURIP Award FA9550-12-1-0016. We thank Jeff Fessler for suggesting the gradient descent method so that the advantage of the steepest descent based method could be properly showcased.

A. Solving Eq. (14) in MATLAB

Specifically, the solution to Eq. (14) can be computed in MATLAB using the CVX package [13,15] by invoking the following sequence of commands:

```
cvx_begin sdp
    variable A(M,M) hermitian
    minimize trace(S11'*S11*A)
    subject to
        A >= 0;
        diag(A) == ones(M,1)/M;
cvx_end
Asdp = A; % return optimum in variable Asdp
```

For settings where $M > 100$, we recommend using the SDPT3 solver [38]. The solution to Eq. (14) can be computed in MATLAB using the SDPT3 package by invoking the following sequence of commands:

```
cost_function = S11'*S11;
e = ones(M,1); b = e/M;
num_params = M*(M-1)/2;
C{1} = cost_function;
A = cell(1,M); for j = 1:M, A{j} = sparse(j,j,1,M,M); end
blk{1,1} = 's'; blk{1,2} = M; Avec = svec(blk(1,:),A,1);
```

```
[obj,X,y,Z] = sqlp(blk,Avec,C,b);
Asdp = cell2mat(X); % return optimum in variable Asdp
```

B. Derivation of Eq. (45)

Here, we derive Eq. (45). For notational brevity, we replace S_{11} with B , and denote B 's m th row and n th column element as B_{mn} . We will show that

$$\frac{\partial \|B \cdot \underline{p}(\underline{\theta})\|_2^2}{\partial \underline{\theta}} = 2 \operatorname{Im} [\operatorname{diag}\{\underline{p}(-\underline{\theta})\} \cdot B^H \cdot B \cdot \underline{p}(\underline{\theta})]. \quad (\text{A1})$$

To this end, note that the cost function can be expanded as

$$\begin{aligned} \|B \cdot \underline{p}(\underline{\theta})\|_2^2 &= \sum_{n=1}^M |B_{nm} e^{j\theta_m}|^2 \\ &= \sum_{n=1}^M \sum_{m=1}^M |B_{nm}|^2 + 2 \sum_{n=1}^M \sum_{p>q}^M \operatorname{Re} (B_{np} B_{nq}^* e^{j(\theta_p - \theta_q)}) \\ &= \sum_{n=1}^M \sum_{m=1}^M |B_{nm}|^2 + 2 \sum_{n=1}^M \sum_{p>q}^M |B_{np}| |B_{nq}| \cos(\theta_p - \theta_q + \angle B_{np} - \angle B_{nq}), \end{aligned} \quad (\text{A2})$$

where $\operatorname{Re}(\cdot)$ denotes the operator that returns the real part of the argument.

Consequently, the derivative of the cost function with respect to the k th phase θ_k can be expressed as

$$\frac{\partial \|B \cdot \underline{p}(\underline{\theta})\|_2^2}{\partial \theta_k} = -2 \sum_{n=1}^M \sum_{q \neq k}^M \operatorname{Im} [B_{nk} B_{nq}^* e^{j(\theta_k - \theta_q)}] \quad (\text{A3})$$

$$= -2 \operatorname{Im} \left[e^{j\theta_k} \sum_{n=1}^M B_{nk} \sum_{q \neq k}^M B_{nq}^* e^{-j\theta_q} \right], \quad (\text{A4})$$

where $\operatorname{Im}(\cdot)$ denotes the operator that returns the imaginary part of the argument.

Let \underline{e}_k be the k -th elementary vector. We may rewrite Eq. (A4) as

$$\frac{\partial \|B \cdot \underline{p}(\underline{\theta})\|_2^2}{\partial \theta_k} = -2 \operatorname{Im} \left[e^{j\theta_k} \begin{bmatrix} B_{1k} & \cdots & B_{Mk} \end{bmatrix} \cdot B^* \cdot \{I - \underline{e}_k \cdot \underline{e}_k^H\} \cdot \underline{p}(\underline{\theta})^* \right], \quad (\text{A5})$$

or, equivalently, as

$$\frac{\partial \|B \cdot \underline{p}(\underline{\theta})\|_2^2}{\partial \theta_k} = -2 \operatorname{Im} \left[e^{j\theta_k} \begin{bmatrix} B_{1k} & \cdots & B_{Mk} \end{bmatrix} \cdot B^* \cdot \underline{p}(\underline{\theta})^* \right] - 2 \operatorname{Im} \left[\begin{bmatrix} B_{1k} & \cdots & B_{Mk} \end{bmatrix} \cdot B^* \cdot \underline{e}_k \right] \quad (\text{A6})$$

$$= -2 \operatorname{Im} \left[e^{j\theta_k} \begin{bmatrix} B_{1k} & \cdots & B_{Mk} \end{bmatrix} \cdot B^* \cdot \underline{p}(\underline{\theta})^* \right]. \quad (\text{A7})$$

Stacking the elements into a vector yields the relation

$$\frac{\partial \|B \cdot \underline{p}(\underline{\theta})\|_2^2}{\partial \underline{\theta}} = -2 \operatorname{Im} [\operatorname{diag}\{\underline{p}(\underline{\theta})\} \cdot B^T \cdot B^* \cdot \underline{p}(\underline{\theta})^*], \quad (\text{A8})$$

or, equivalently, Eq. (A1).

References

1. J. Aulbach, B. Gjonaj, P. M. Johnson, A. P. Mosk, and A. Lagendijk. Control of light transmission through opaque scattering media in space and time. *Physical review letters*, 106(10):103901, 2011.
2. C. Barnes and J. B. Pendry. Multiple scattering of waves in random media: a transfer matrix approach. *Proceedings of the Royal Society of London. Series A: Mathematical and Physical Sciences*, 435(1893):185, 1991.
3. C. W. J. Beenakker. Applications of random matrix theory to condensed matter and optical physics. *Arxiv preprint arXiv:0904.1432*, 2009.
4. T. Chaigne, J. Gateau, O. Katz, E. Bossy, and S. Gigan. Light focusing and two-dimensional imaging through scattering media using the photoacoustic transmission matrix with an ultrasound array. *Optics Letters*, 39(9):2664–2667, 2014.
5. W. Choi, A. P. Mosk, Q.-H. Park, and W. Choi. Transmission eigenchannels in a disordered medium. *Physical Review B*, 83(13):134207, 2011.
6. M. Cui. A high speed wavefront determination method based on spatial frequency modulations for focusing light through random scattering media. *Optics Express*, 19(4):2989–2995, 2011.
7. M. Cui. Parallel wavefront optimization method for focusing light through random scattering media. *Optics letters*, 36(6):870–872, 2011.
8. O. N. Dorokhov. Transmission coefficient and the localization length of an electron in N bound disordered chains. *JETP Lett*, 36(7), 1982.
9. T. J. Dougherty, C. J. Gomer, B. W. Henderson, G. Jori, M. Kessel, D. and Korbelik, J. Moan, and Q. Peng. Photodynamic therapy. *Journal of the National Cancer Institute*, 90(12):889–905, 1998.
10. C. Forbes, M. Evans, N. Hastings, and B. Peacock. *Statistical distributions*. John Wiley & Sons, 2011.
11. M. Goemans and D. P. Williamson. Improved approximation algorithms for maximum cut and satisfiability problems using semidefinite programming. *Journal of the ACM (JACM)*, 42(6):1115–1145, 1995.
12. G. H. Golub and C. F. Van Loan. *Matrix computations*. JHU Press, Fourth edition, 2012.

13. M. Grant and S. Boyd. Graph implementations for nonsmooth convex programs. In V. Blondel, S. Boyd, and H. Kimura, editors, *Recent Advances in Learning and Control*, Lecture Notes in Control and Information Sciences, pages 95–110. Springer-Verlag Limited, 2008. http://stanford.edu/~boyd/graph_dcp.html.
14. R. A. Horn and C. R. Johnson. *Matrix analysis*. Cambridge university press, 1990.
15. CVX Research Inc. CVX: Matlab software for disciplined convex programming, version 2.0. <http://cvxr.com/cvx>, August 2012.
16. A. Ishimaru. *Wave propagation and scattering in random media*. IEEE/OUP Series on Electromagnetic Wave Theory. IEEE Press, New York, 1997. Reprint of the 1978 original, With a foreword by Gary S. Brown, An IEEE/OUP Classic Reissue.
17. C. Jin, R. R. Nadakuditi, E. Michielssen, and S. Rand. An iterative, backscatter-analysis based algorithm for increasing transmission through a highly-backscattering random medium. In *Statistical Signal Processing Workshop (SSP), 2012 IEEE*, pages 97–100. IEEE, 2012.
18. C. Jin, R. R. Nadakuditi, E. Michielssen, and S. Rand. Iterative, backscatter-analysis algorithms for increasing transmission and focusing light through highly scattering random media. *JOSA A*, 30(8):1592–1602, 2013.
19. M. Kim, Y. Choi, C. Yoon, W. Choi, J. Kim, Q.-Han. Park, and W. Choi. Maximal energy transport through disordered media with the implementation of transmission eigenchannels. *Nature Photonics*, 6(9):583–587, 2012.
20. T. W. Kohlgraf-Owens and A. Dogariu. Transmission matrices of random media: Means for spectral polarimetric measurements. *Optics letters*, 35(13):2236–2238, 2010.
21. F. Kong, R. H. Silverman, L. Liu, P. V. Chitnis, K. K. Lee, and Y-C. Chen. Photoacoustic-guided convergence of light through optically diffusive media. *Optics letters*, 36(11):2053–2055, 2011.
22. M. Ledoux. *The concentration of measure phenomenon*, volume 89. American Mathematical Soc., 2005.
23. Z.-Q. Luo, W.-K. Ma, A. M.-C. So, Y. Ye, and S. Zhang. Semidefinite relaxation of quadratic optimization problems. *Signal Processing Magazine, IEEE*, 27(3):20–34, 2010.
24. R. C. McPhedran, L. C. Botten, A. A. Asatryan, N. A. Nicorovici, P. A. Robinson, and C. M. De Sterke. Calculation of electromagnetic properties of regular and random arrays of metallic and dielectric cylinders. *Physical Review E*, 60(6):7614, 1999.
25. P. A. Mello, P. Pereyra, and N. Kumar. Macroscopic approach to multichannel disordered conductors. *Annals of Physics*, 181(2):290–317, 1988.
26. Y. Nesterov. Semidefinite relaxation and nonconvex quadratic optimization. *Optimization methods and software*, 9(1-3):141–160, 1998.
27. Y. Nesterov, H. Wolkowicz, and Y. Ye. Semidefinite programming relaxations of noncon-

- vex quadratic optimization. In *Handbook of semidefinite programming*, pages 361–419. Springer, 2000.
28. J. B. Pendry, A. MacKinnon, and A. B. Pretre. Maximal fluctuations—a new phenomenon in disordered systems. *Physica A: Statistical Mechanics and its Applications*, 168(1):400–407, 1990.
 29. S. M. Popoff, G. Lerosey, R. Carminati, M. Fink, A. C. Boccarda, and S. Gigan. Measuring the transmission matrix in optics: an approach to the study and control of light propagation in disordered media. *Physical review letters*, 104(10):100601, 2010.
 30. C. R. Rao. *Linear statistical inference and its applications*. John Wiley & Sons, New York-London-Sydney, second edition, 1973. Wiley Series in Probability and Mathematical Statistics.
 31. Z. Shi, J. Wang, and A. Z. Genack. Measuring transmission eigenchannels of wave propagation through random media. In *Frontiers in Optics*. Optical Society of America, 2010.
 32. M. M. Siddiqui. Some problems connected with rayleigh distributions. *Journal of Research of the National Bureau of Standards*, 660:167–174, 1962.
 33. A. Sidi. *Practical extrapolation methods*, volume 10 of *Cambridge Monographs on Applied and Computational Mathematics*. Cambridge University Press, Cambridge, 2003. Theory and applications.
 34. S. Singh and R. Singh. On the use of Shank’s transform to accelerate the summation of slowly converging series. *Microwave Theory and Techniques, IEEE Transactions on*, 39(3):608–610, 1991.
 35. S. T. Smith. Optimum phase-only adaptive nulling. *Signal Processing, IEEE Transactions on*, 47(7):1835–1843, 1999.
 36. A. M.-C. So, J. Zhang, and Y. Ye. On approximating complex quadratic optimization problems via semidefinite programming relaxations. *Mathematical Programming*, 110(1):93–110, 2007.
 37. C. Stockbridge, Y. Lu, J. Moore, S. Hoffman, R. Paxman, K. Toussaint, and T. Bifano. Focusing through dynamic scattering media. *Optics Express*, 20(14):15086–15092, 2012.
 38. K. H. Toh, M. J. Todd, and R. H. Tutuncu. SDPT3 version 4.0 – a MATLAB software for semidefinite-quadratic-linear programming.
 39. L. N. Trefethen and D. Bau III. *Numerical linear algebra*. Number 50. Society for Industrial Mathematics, 1997.
 40. E. G. van Putten, A. Lagendijk, and A. P. Mosk. Optimal concentration of light in turbid materials. *JOSA B*, 28(5):1200–1203, 2011.
 41. E. G. van Putten, I. M. Vellekoop, and A. P. Mosk. Spatial amplitude and phase modulation using commercial twisted nematic lcds. *Applied optics*, 47(12):2076–2081, 2008.

42. L. Vandenberghe and S. Boyd. Semidefinite programming. *SIAM review*, 38(1):49–95, 1996.
43. I. M. Vellekoop and A. P. Mosk. Phase control algorithms for focusing light through turbid media. *Optics Communications*, 281(11):3071–3080, 2008.
44. I. M. Vellekoop and A. P. Mosk. Universal optimal transmission of light through disordered materials. *Physical review letters*, 101(12):120601, 2008.
45. X. Wang, W. W. Roberts, P. L. Carson, D. P. Wood, and B. J. Fowlkes. Photoacoustic tomography: a potential new tool for prostate cancer. *Biomedical optics express*, 1(4):1117–1126, 2010.
46. S. Zhang and Y. Huang. Complex quadratic optimization and semidefinite programming. *SIAM Journal on Optimization*, 16(3):871–890, 2006.

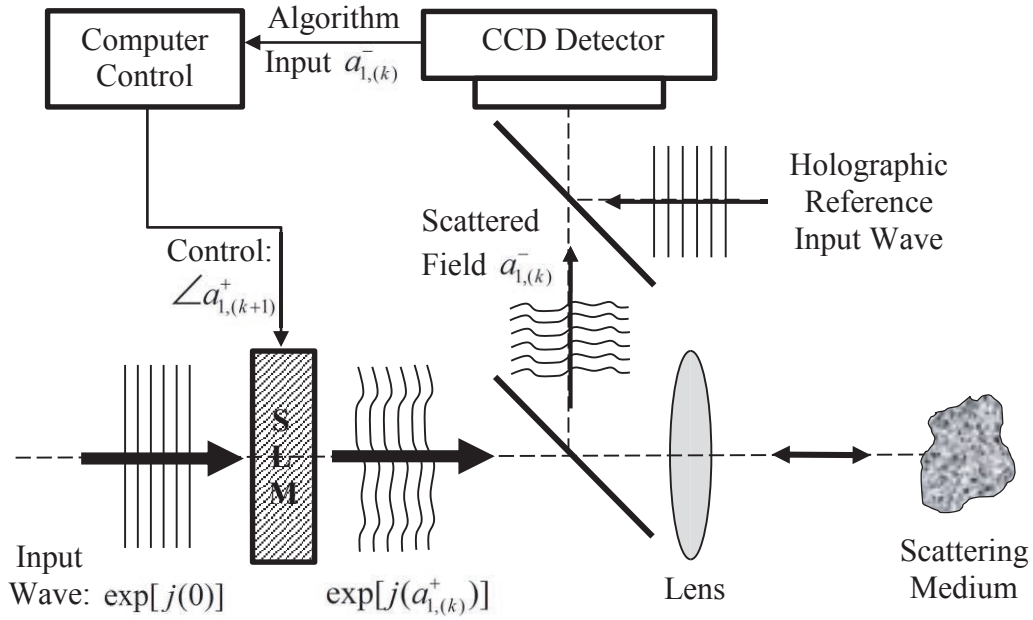


Fig. 1. Schematic for the experimental setup considered.

- Periodic repetition
- with period D

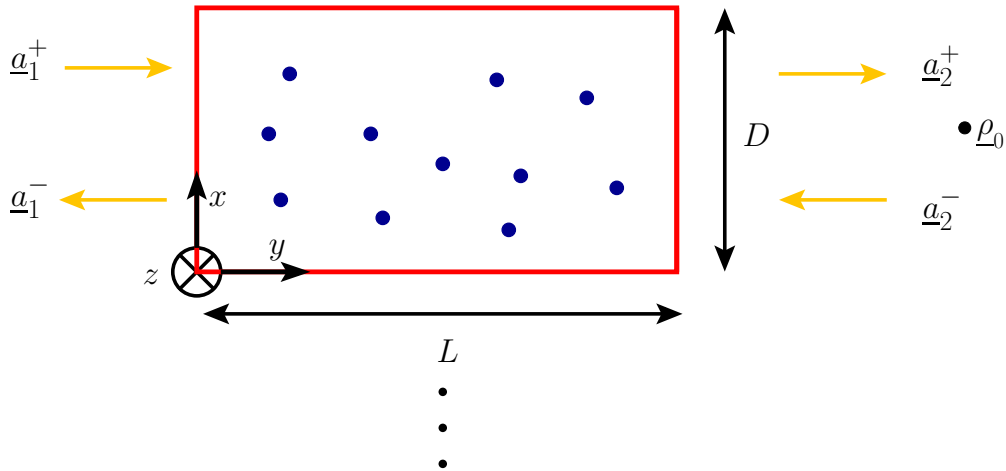


Fig. 2. Geometry of the scattering system considered.

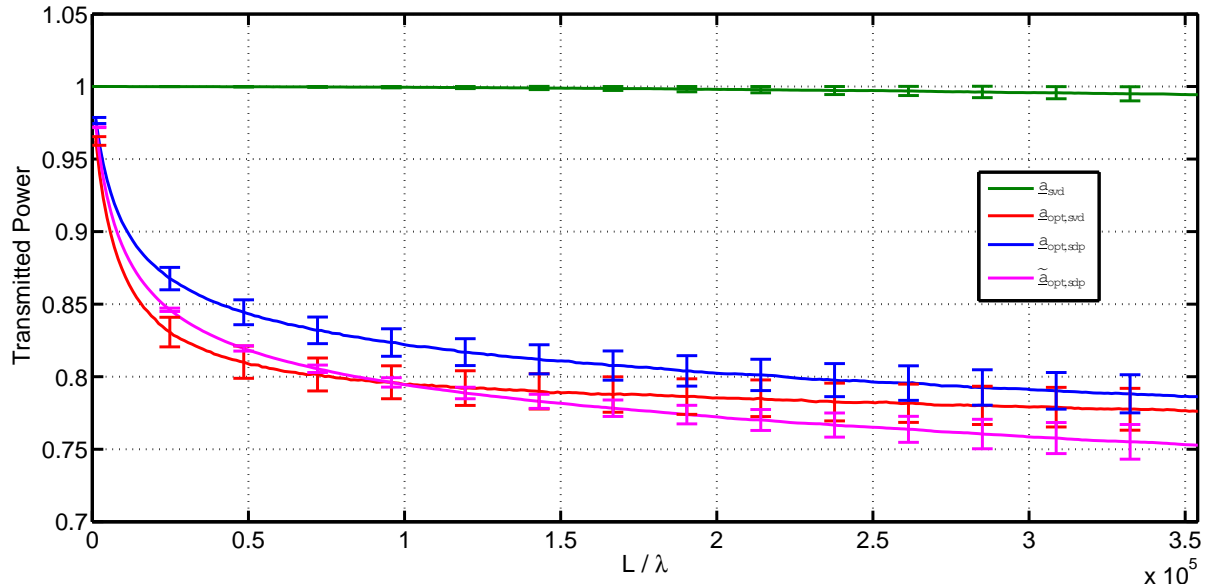


Fig. 3. Plot of transmitted power obtained by the SVD and SDP based algorithms versus L/λ in a setting where $D = 197\lambda$, $r = 0.11\lambda$, $n_d = 1.3$ and $M = 395$. The system was generated so that when $L = 3.4 \times 10^5\lambda$, $N_c = 430,000$ and $\bar{l} = 6.69\lambda$, where \bar{l} is the average distance to the nearest scatterer. The empirical average and the one-standard-deviation error bars were computed over 1700 random realizations of the scattering medium.

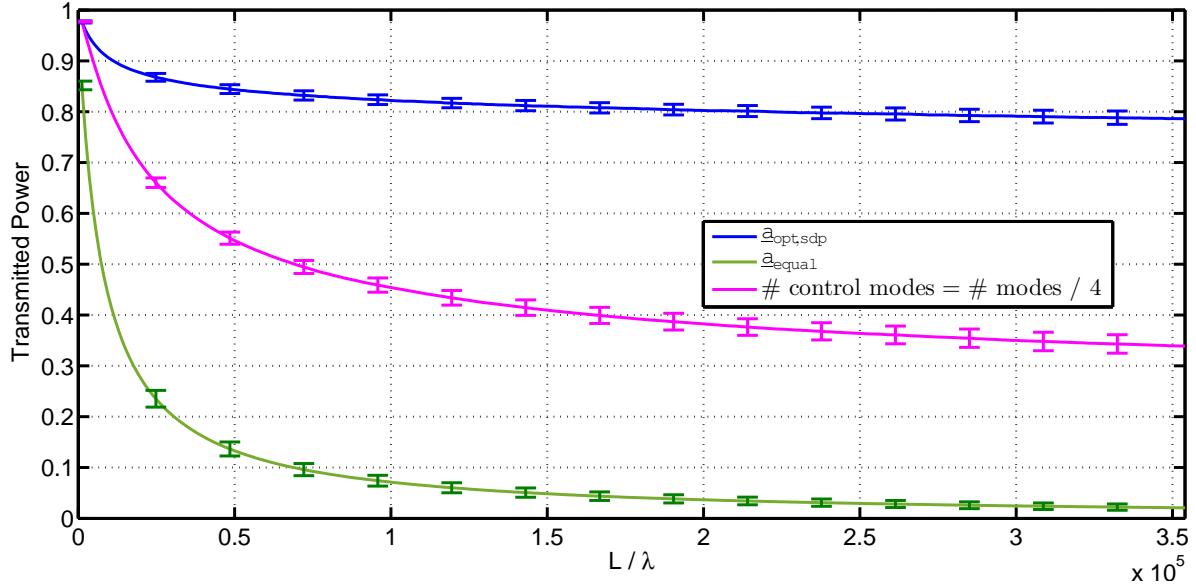


Fig. 4. Plot of transmitted power obtained by the $a_{\text{opt,sdp}}$, a_{equal} and the amplitude and phase modulated wavefront corresponding to the largest right singular vector of the undersampled (by four) modal transmission matrix versus L/λ for the same setup as in Fig. 3.

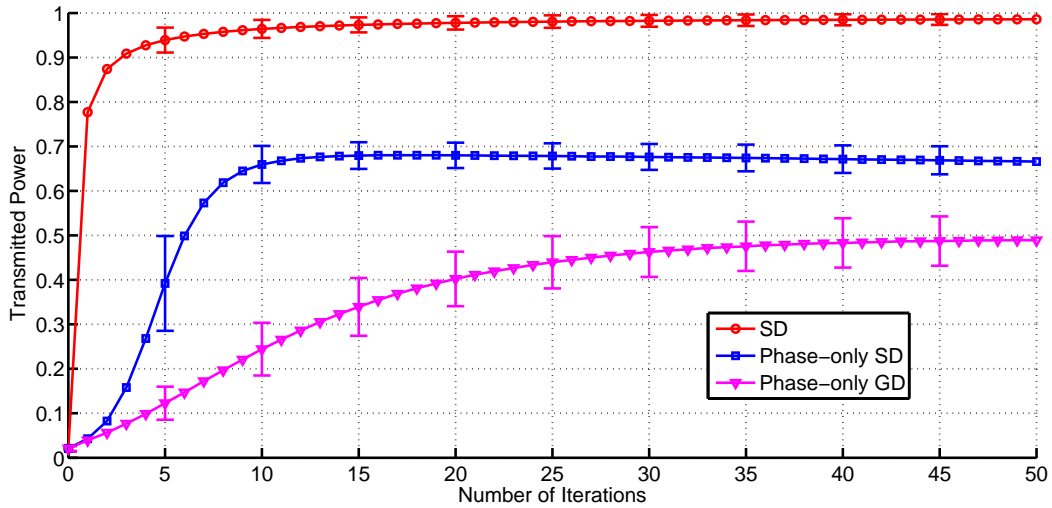


Fig. 5. The average transmitted power versus the number of iterations is shown for steepest descent algorithm, the phase-only steepest descent algorithm and the phase-only gradient descent algorithm for setup described in Fig. 3. Here $L = 3.4 \times 10^5 \lambda$. For each of these algorithms the optimal step size μ was chosen by a line search.

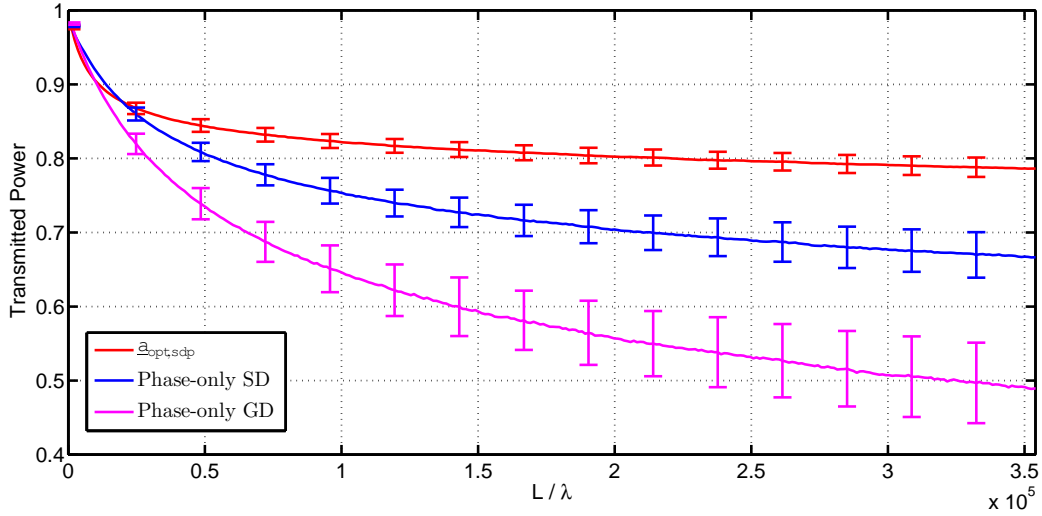


Fig. 6. The average transmitted power obtained after 50 iterations of the phase-only steepest descent (SD) and gradient descent (GD) methods as a function of L/λ for the setup described in Fig. 3. For comparison, we plot the transmitted power realized by $a_{\text{opt,sdp}}$.

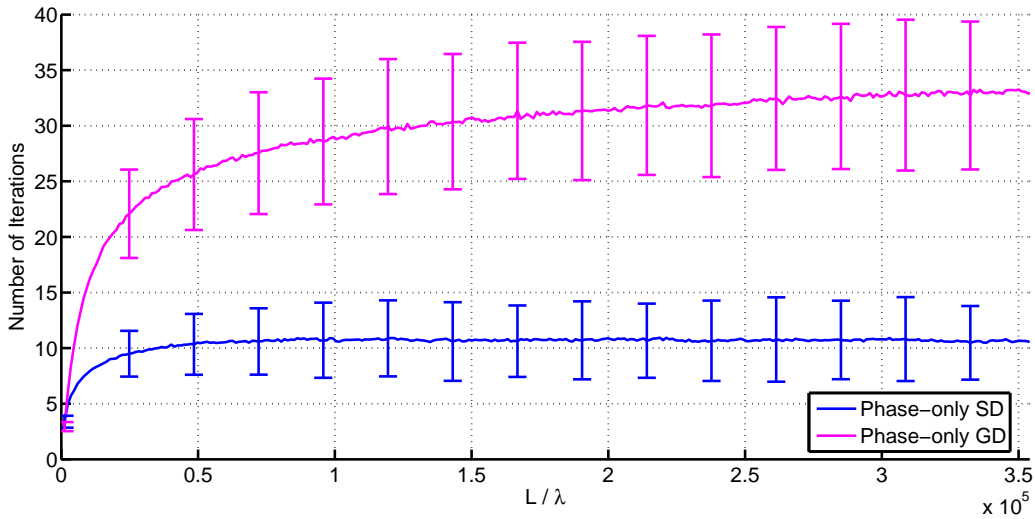


Fig. 7. Average number of iterations to get to 95% of the respective maximum transmitted power for the phase-only steepest descent and gradient descent algorithms as a function of L/λ for the setup described in Figure 3.

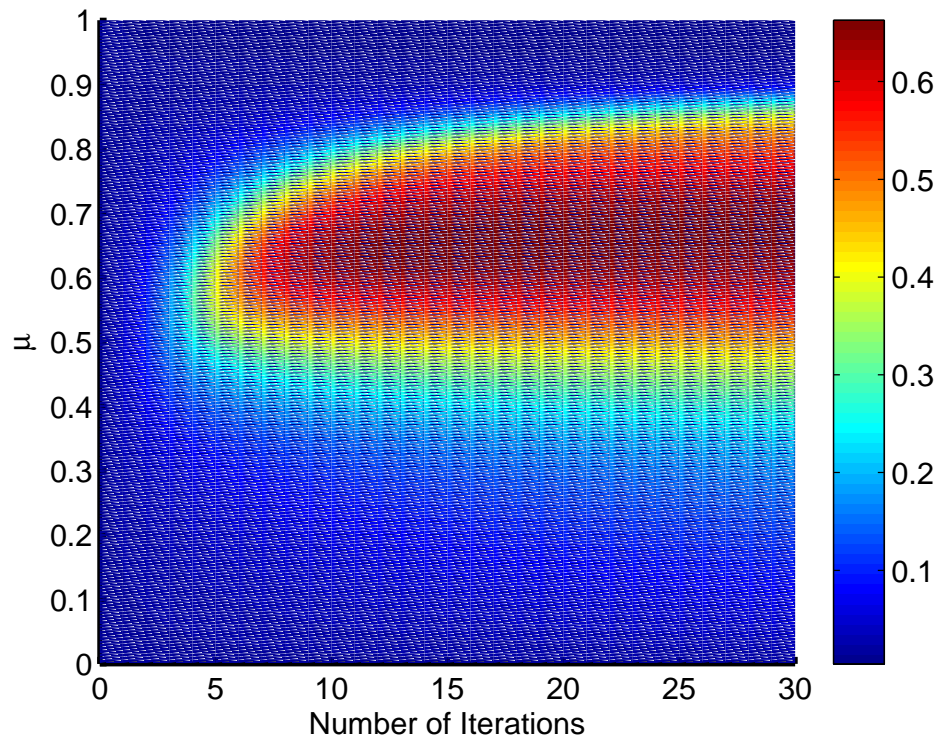


Fig. 8. Heatmap of the average transmitted power attained by the phase-only steepest descent algorithm as a function of the number of iterations and stepsize μ for the same setup as in Fig. 5.

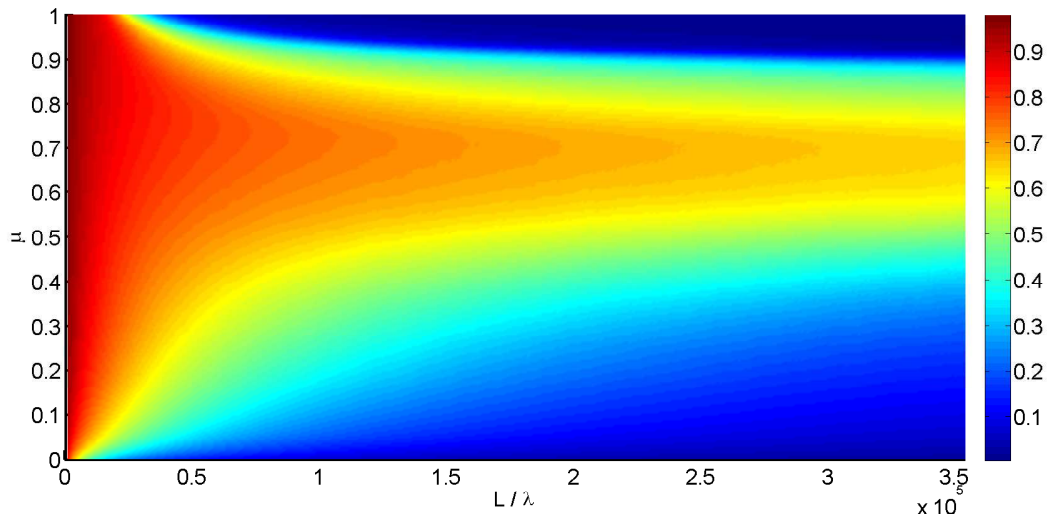


Fig. 9. Heatmap of the maximum transmitted power in 50 iterations of steepest descent on the plane of stepsize and the thickness L/λ for the setup in Figure 3.

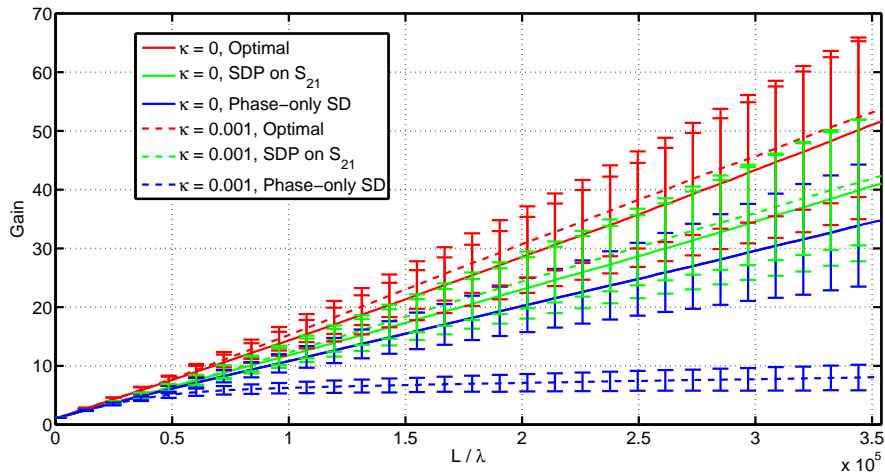


Fig. 10. Gain in transmitted power relative to a_{equal} versus thickness L/λ for a system setup as described in Fig. 3 except with $n_d = 1.3 - j\kappa$, where κ is the extinction coefficient.